ChemEngineering

Article

Frequencies, Velocities, and Spacing of Interfacial Waves of Falling Liquid Films in a Large Diameter Vertical Pipe

Abbas H Hasan [1,*], Shara K Mohammed [2], Buddhika Hewakandamby [3], Faiza Saidj [4], Abdelwahid Azzi [4] and Barry James Azzopardi [3,†]

[1] Faculty of Engineering, University of Hull, Hull HU67RX, UK
[2] Department of Petroleum Technology, Erbil Technology College, Erbil Polytechnic University, Erbil 44001, Iraq
[3] Faculty of Engineering, University of Nottingham, University Park, Nottingham NG72RD, UK
[4] Faculty of Mechanical and Process Engineering, Université des Sciences et de la Technologie Houari Boumediène, BP 32 El Alia, Algiers 16111, Algeria
* Correspondence: a.hasan@hull.ac.uk
† Deceased Author.

Abstract

Many of the film thickness measurements that have been reported in the literature tend to focus on small pipe diameters, which may not be practical for a variety of industrial applications. Additionally, single-point measurements are unable to provide the necessary film thickness data around the circumference of the pipe as well as in the axial direction. This paper aims to experimentally study the behaviour of wavy liquid films, including wave frequency, wave velocity, wave width, and wave spacing. A Multi-Pin Film Sensor (MPFS) was used to extract the thickness of a free-falling liquid film in axial, circumferential, and temporal coordinates. The range of liquid Reynolds number Re_L used was 618–1670. It was found that the power spectral density of the disturbance waves showed a pronounced peak at the modal frequency of 6–8 Hz. The number of disturbance waves was found to be almost independent of Re_L. The axial interfacial wave seemed to travel at a constant velocity while the mean velocity in circumferential direction was negligible. The mean width of the disturbance waves was approximately 17.7% of the pipe diameter.

Keywords: falling liquid film; interfacial waves; wave frequency; wave spacing; wave width

1. Introduction

Liquid films in pipes can be found in various low and high viscous gas–liquid two-phase flows [1–5]. However, it can also exist in the absence of the gas flow. Falling films under the influence of gravity are found in many process equipment and industrial applications such as evaporators, condensers, heat exchangers, reactors, and wetted-wall columns/plates. Falling liquid films have random interfacial waviness behaviour which significantly affects the flow momentum as well as heat and mass transfer, even without interfacial shear stresses caused by the gas flow [6–8]. Therefore, to design such equipment in a more efficient, safe, and economic way, an in-depth understanding of the wave dynamics and its structure is required. Considerable experimental and theoretical studies on falling liquid films have been reported in the literature. These include, Telles and Dukler [9]; Gjevik [10]; Dukler [7]; Karapantsios et al. [11]; Zadrazil et al. [12]; Gerke and Repke [13]; and Zeng et al. [14]. Karapantsios et al. [11] investigated the flow behaviour of freely liquid falling films in a 50 mm pipe diameter using two single-point film thickness measurements

Check for updates

Academic Editor: José P. Coelho

Received: 29 October 2025
Revised: 25 December 2025
Accepted: 12 January 2026
Published: 24 February 2026

Copyright: © 2026 by the authors. Licensee MDPI, Basel, Switzerland. This article is an open access article distributed under the terms and conditions of the Creative Commons Attribution (CC BY) license.

with Re_L ranging from 509 to 13,090. The distance between the inlet and the sensor was 2.55 m. They reported that the spectral density function PSD of the film thickness exhibits a modal frequency (corresponds to the disturbance wave) between 5 Hz and 8 Hz. This modal frequency seems, practically, independent of the liquid Reynolds number.

Meza and Balakotaiah [15] conducted experimental work using a long test section of 5.23 m with a diameter of 0.076 m to correlate the large waves amplitude of the falling film to the Weber number. They found that the large waves (i.e., at low frequencies) generated far from the inlet are formed in packets with a velocity of approximately 3 m/s. In addition, merging and splitting of the waves as they move downward were reported and at the end of waves interaction period (where the wave spacing becomes far enough), the amplitudes of the disturbance waves are approximately close to each other. Yu et al. [16] found that the waves in the freely falling film (beyond 2.74 m from the entrance) move approximately with the same velocity. Similar observation was observed by Drosos et al. [17] who also reported that the axial velocity of the wave increases as the liquid Reynolds number Re_L increases and the large waves move faster in the falling film. They classified the wave evolution in the freely falling film into three distinct regions. The first region shows very strong dependence of wave amplitude on Re_L (particularly, at low Re_L), where the wave fronts grow in magnitude in the lateral direction. The second region (at moderate liquid Reynolds number) shows a growth in wavelength, speed, and amplitude of the waves downstream. In the third region (where Re_L > ~200), the waves show a tendency of becoming nearly independent of the liquid flow rate where the amplitude of the waves tend to be constant. Karapantsios et al. [11] found that the large interfacial waves travel with a velocity faster than the liquid film and at Re_L = 6700, two dimensional waves appear in which their fronts occupy a large portion the tube circumference. The study showed that at $Re_L \geq 400$, the measured mean film thickness data starts to deviate significantly from Nusselt data. In addition, at $Re_L < 1250$, the magnitude of the disturbance waves increases. Moreover, the frequency as well as the amplitude of disturbance waves are found almost constant when the Re_L exceeds 1250. The longitudinal behaviour of wavy falling film was investigated by Karapantsios and Karabelas [18] who reported that the streamwise wave velocity tends to increase with axial distance, particularly at low Re_L. Karimi and Kawaji [19] studied, experimentally, the dynamic characteristics of freely falling film using a 50.80 mm diameter pipe (with $1408 < Re_L < 6549$) and found that the measured velocity profiles significantly deviate from Nusselt's correlation in wavy/turbulent freely falling films, but it was matched well with flat films (at low Re_L). The study by Zeng et al. [14] who investigated the turbulent falling liquid film thickness distribution (using Re_L in the range of 8460–25,900) reported that increasing Re_L can accelerate the large waves velocity causing more collisions and merges between the waves which, in turn, leads to liquid film rapture. They also found that critical liquid film rapture velocity decreases with the decreasing curvature of the plate. Pavlov et al. [20] and Chao et al. [21] showed that increasing Re_L leads to increasing velocity and frequency of the large waves (and hence, increasing the energy accumulation) which can intensify the deformation degree of the liquid film.

Kondo et al. [22] found that the width of the wave increases as the liquid flow rate increases. At higher Re_L (where disturbance waves form), the widths of the disturbance waves remain almost constant, indicating that the width of the waves becomes independent of Re_L. Hewitt and Nicholls [23] and Pashniak [24] reported that velocities for individual waves depend linearly on the width of the wave. Kondo et al. [22] also showed that the width of the disturbance wave (i.e., axial length) represents 2/3 of the pipe diameter. Azzopardi [25] used the velocity and frequency data to find the disturbance wave spacing. He found that the wave spacing decreases with increasing liquid superficial velocity (or Re_L) and the relationship between the mean film thickness and the wave spacing is not correlated.

Conductivity probes were extensively used to measure the liquid film thickness [26–28]. Chu and Dukler [29] used four axial planes, each with four conductive sensors (90° apart around the pipe circumference) to measure and analyze the statistical behaviour of the wave structure and substrate thickness in downward flows using 50.8 mm ID and 4.27 m long vertical pipe. Karapantsios et al. [11] used two parallel conductance wire probes (180° apart in circumferential direction) to measure the film thickness in a 50 mm diameter pipe. Hewitt and Lovegrove [30] used four conductance sensors (90° apart around pipe circumference, using 32 mm pipe diameter) to measure the film thickness of gas–liquid two-phase flows.

Most of the studies in the literature used either single-point measurement (which might not be able to provide a full film thickness measurement, both axially and circumferentially) or small pipe diameters which are not realistic, particularly for industrial applications. Wavy falling liquid films which can be found in many applications and equipment (such as evaporators, condensers, and other wetted-wall columns) can significantly affect the mass/heat and momentum transfers. Optimizing the performance of these units is crucial for minimizing carbon footprint and energy consumption. Therefore, it is important to thoroughly understand the dynamic behaviour of the interfacial falling films for safe, economic, and efficient design of such equipment. In this study, a unique Multi-Pin Film Sensor, MPFS, was used to comprehensively measure and analyze film thickness in three different coordinates: time, circumferential, and axial. The purpose was to provide detailed experimental characterization of interfacial wave properties, including frequency, velocity, spacing, and width, in a freely falling liquid film using a pipe with a 127 mm diameter. The experimental data in this study was also compared with the work of Chu and Dukler [31], who employed a 50.8 mm diameter pipe, to examine the impact of pipe diameter on wave frequency, velocity, width, and amplitude. The experimental results presented in this study could be highly beneficial for modellers, providing a reliable basis for validating models, particularly those involving large pipe diameters.

2. Materials and Methods

The flow facility of the falling film is shown in Figure 1. Water is pumped to the test section (127 mm diameter) through a rotameter and a liquid film distributor at the top section of the pipe. A Multi-Pin Film Sensor (MPFS), which is located 3.5 m downstream of the distributor, was used to measure the liquid film thickness. This unique MPFS consists of 10 axial planes, each containing 64 pin probes in the circumferential direction, see Figure 1. It can extract the three-dimensional (time, axial, and circumferential) data of the liquid film thickens with a high temporal resolution of 1000 Hz. The spatial resolutions in circumferential and axial directions are 6.234×10^{-3} m and 0.0154 m, respectively. This MPFS is quite similar to that used by [26]. However, the latter used a smaller pipe dimeter with different shapes and configurations of the pin probes. During the calibration process, different diameters of non-conducting rods were inserted inside the MPFS. The water film thickness was then measured for each pin sensor (or receiver). In this study, 64 circumferential conductance pin receivers and 9 axial planes were used. In other words, 576 film thickness measurements can be obtained. Sensor calibration was performed by inserting non-conductive inserts of varying diameters into a water-filled annulus to represent different film thicknesses. The liquid temperature was maintained at approximately 22 °C for all experimental runs. Accordingly, three calibration trials were conducted for each receiver at a constant temperature of 22 °C. A sample calibration curve for a single receiver, with standard error is shown in Figure 2, where ADC represents the Analogue to Digital Converter unit in the electrical circuit of the MPFS.

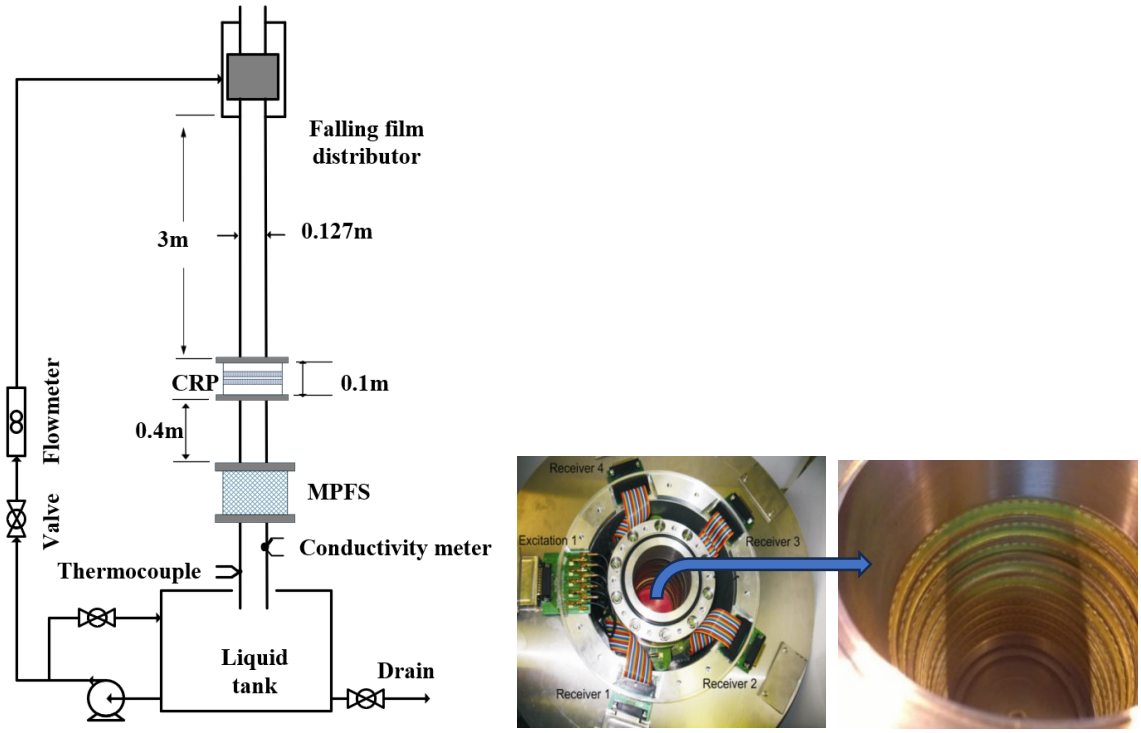

Figure 1. (**left**) Flow facility of the falling liquid film. (**right**) MPFS probes from inside with 640 pin probes [32].

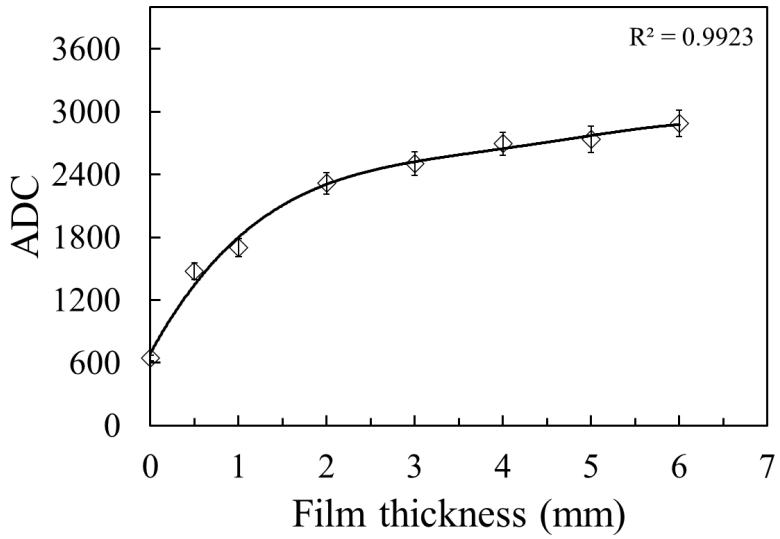

Figure 2. Calibration curve of the MPFS.

The average circumferential film thickness obtained by the first plane of the MPFS was compared with the data obtained from the conductance-ring probe (CRP) for validation, as shown in Figure 3. The results showed good agreement between the two methods. A comparison was also made between the two local film thickness measurements using a single receiver of MPFS and ultrasonic sensor [2], both local measurements results showed good agreement as illustrated in Figure 3.

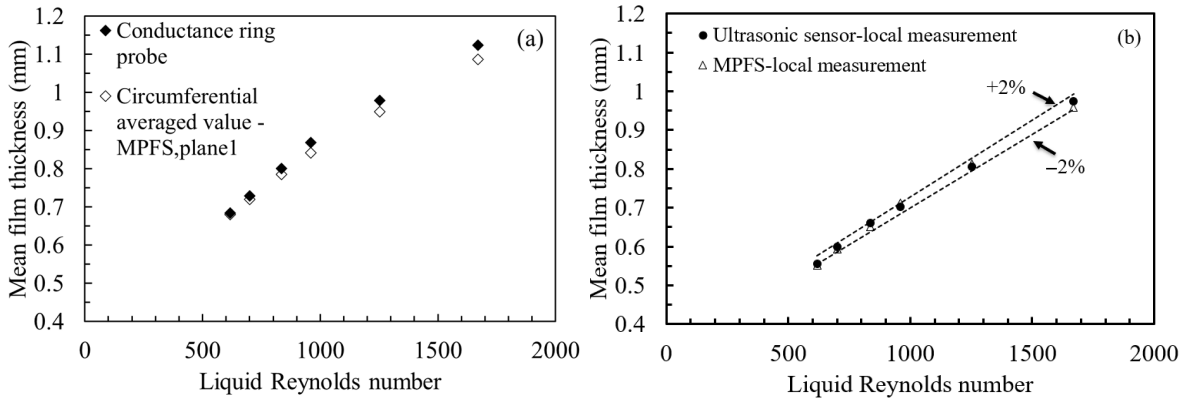

Figure 3. Comparison of (**a**) MPFS with CRP and (**b**) MPFS with ultrasonic sensor.

The range of the liquid Reynolds number was 618 to 1670. The liquid Reynolds number is given by

$$Re_L = \frac{4\Gamma}{\mu} \quad (1)$$

where Γ and μ are the mass flow rate of the liquid (per wetted-perimeter) and the dynamic viscosity of the liquid, respectively.

3. Results and Discussion

3.1. Frequency of the Wave

The power spectral density (PSD) is a powerful statistical tool to identify the frequency of the most dominant feature (e.g., disturbance wave) of the flow [12,33,34]. Figure 4 shows the PSD at low, moderate, and high Re_L, respectively. The PSD is represented in dB. All PSD functions exhibit a pronounced peak at a modal frequency of 6 to 8 Hz. These modal frequencies correspond to the large ordisturbance waves and they can be practically considered as independent of Re_L [12]. However, it is found from Figure 4 that the modal frequencies at low and moderate Re_L (i.e., Re_L = 618 and 960) are 6 Hz while at higher Re_L (i.e., Re_L = 1670), the modal frequency tends to move to the right and increases to 8 Hz. As expected, the power spectrum is concentrated at low frequency or in the large amplitude waves [15]. By comparing the current values of the modal frequency with previous studies, Chu and Dukler [31] reported that the modal frequencies of the power spectral density, PSD (for Re_L = 570–7560) were between 2 Hz and 5 Hz. They also reported that their modal frequency increased with increasing Re_L. Takahama and Kato [35] found that for Re_L = 2052, the modal frequency was about 10 Hz, while the modal frequency obtained by Zabaras et al. [36] was 6 Hz for a liquid Reynolds number of 768 and 3100. Karapantsios et al. [11], who used Re_L in the range of 509 to 13,090, found that the modal frequency of the power spectral density lies between 5 and 8 Hz. It is also seen from Figure 4 that at high liquid Reynolds number (Re_L = 1670), second weaker-peaks appeared in the frequency range of 14 to 20 Hz. These second types of frequency can be attributed to the small waves generated between disturbance waves. Karapantsios et al. [11] also reported the same observation.

The calculated frequency obtained by counting the number of waves in the time series of the film thickness was achieved by using different Minimum Peak Prominence (MPP) detecting technique in MATLAB R2024b. Peak prominence represents a peak-to-peak amplitude of the waves. In other words, any wave that has a peak-to-peak amplitude $\geq$ MPP value will only be considered in the counting process (for illustration, see Figure 5 which defines MPP as a 0.5 times the mean film thickness of selected time series). Figure 6 displays the calculated frequency obtained from counting the number of

waves in the film thickness time series at different MPP values. Previous studies, such as those conducted by [26,37], have reported that the height of disturbance waves is typically around four times the average film thickness. Therefore, to study the relationship between wave frequency and liquid Reynolds number in a freely falling film, we defined MPP values by using various threshold factors multiplied by the mean film thickness, $\overline{\delta}$ (i.e., $0.5\overline{\delta}$, $1\overline{\delta}$, $1.5\overline{\delta}$, $2\overline{\delta}$, $3\overline{\delta}$, and $4\overline{\delta}$, respectively). It is clear from Figure 6 that if the MPP increases (i.e., the factor multiplied by the mean film thickness increases), then the frequency decreases due to the decreasing in the number of the waves. The modal values of the PSD of the film thickness are also plotted in Figure 6. It is seen that PSD fits fairly well with the frequency data obtained by waves counting when MPP equals $2\overline{\delta}$, particularly at low to moderate liquid Reynolds number. One can also observe that as the MPP values increase (e.g., at $4\overline{\delta}$, i.e., a typical disturbance wave), the number of the waves become almost independent of the liquid Reynolds number. Similar observation was found by [12] who reported that wave frequencies at a wave amplitude threshold of two times the mean film thickness ($2\overline{\delta}$) becomes more dependent on the Re_L compared to the wave frequencies measured at $3\overline{\delta}$ and $4\overline{\delta}$. Wave frequencies (at $4\overline{\delta}$) are approximately independent of Re_L. Karapantsios et al. [11] also showed that the frequencies of disturbance waves (<10 Hz) are generally independent of the mean liquid flow rate.

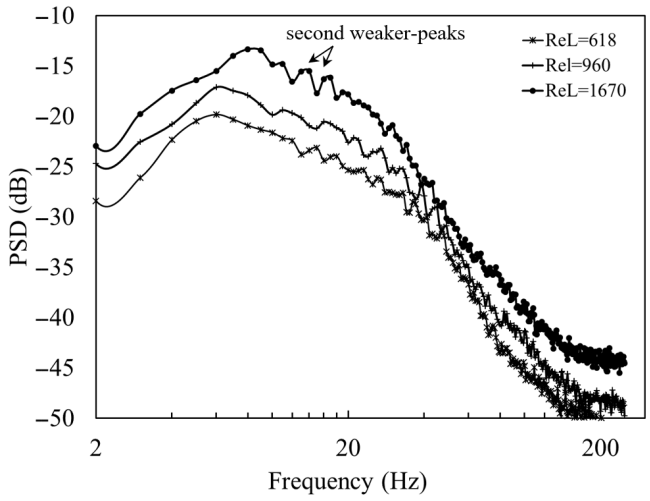

Figure 4. Power spectral density at low, moderate and high liquid Reynolds number.

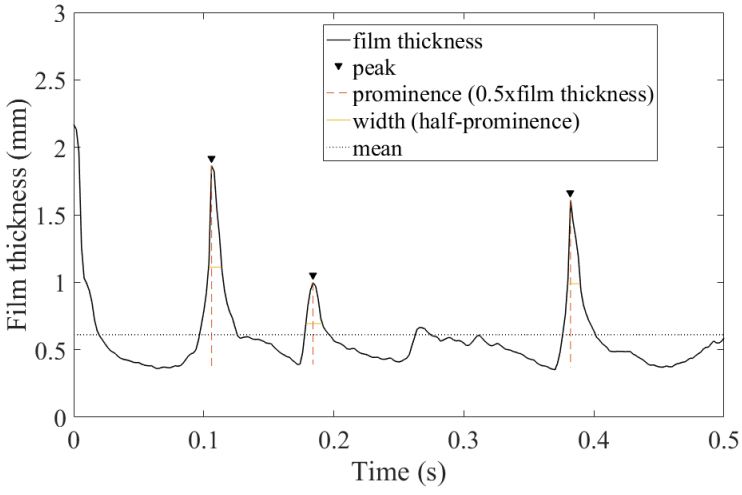

Figure 5. Prominence, peaks, and widths of the waves.

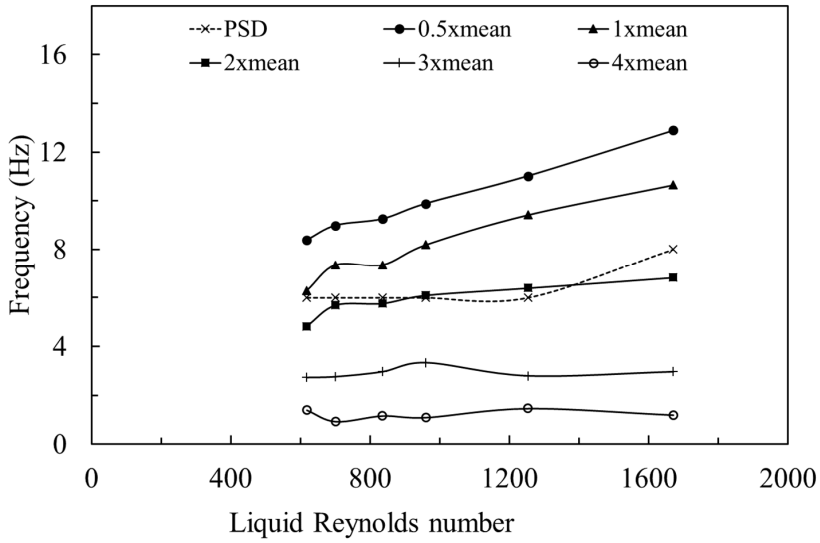

Figure 6. Calculated frequency by counting the number of the waves using different MPP values.

The surface waves at low Reynolds number are controlled by the interaction occurred between the waves and the substrate. Additionally, large waves can change the local Reynolds number, causing more ripples to form due to the strain structure produced by the liquid film [38]. As the Reynolds number increases, the collision between ripple waves becomes more significant. This causes resonance waves generated during the ripples collision to catch up with the front waves resulting in mass accumulation and the formation of large waves [39–41].

In order to demonstrate the impact of pipe diameter on wave frequency, the data collected in this study was compared to the findings of Chu and Dukler [31]. Figure 7 illustrates the wave frequency of the substrate in the current study (with a pipe diameter of 127 mm) and Chu and Dukler's study (with a diameter of 50.8 mm). The results indicate that the substrate experiences fewer waves with a larger pipe diameter than with a smaller one. The wave frequency for the 50.8 mm diameter pipe is approximately 3.5 times greater than that for the 127 mm diameter pipe.

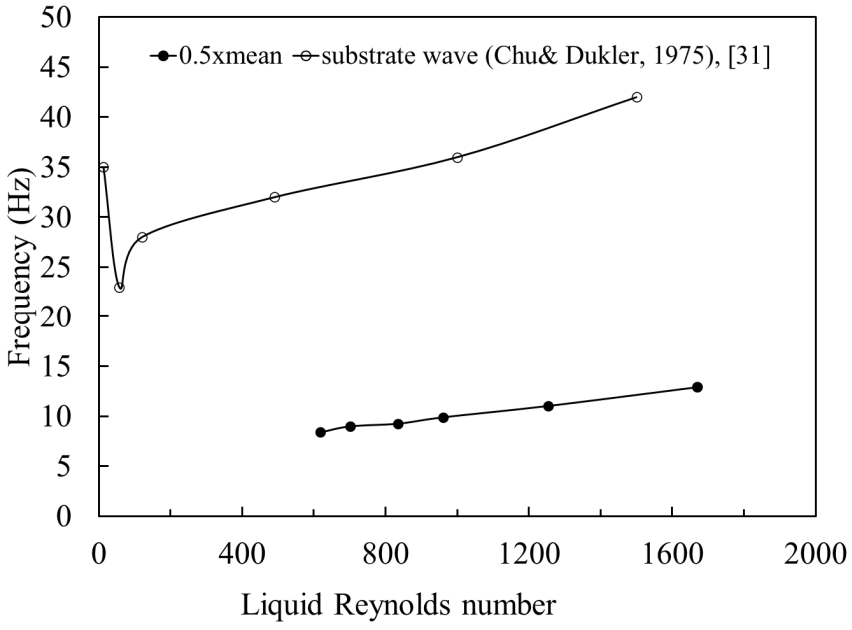

Figure 7. Effect of pipe diameter on substrate frequency.

The frequency of the disturbance-wave in the current study was also compared with disturbance wave frequency of Chu and Dukler [31] as shown in Figure 8, using the dimensionless frequency form of the Strouhal number St which is given by

$$St = \frac{fD}{U_{ls}} \quad (2)$$

where f is the wave frequency, D is the pipe diameter, and U_{ls} is the liquid superficial velocity.

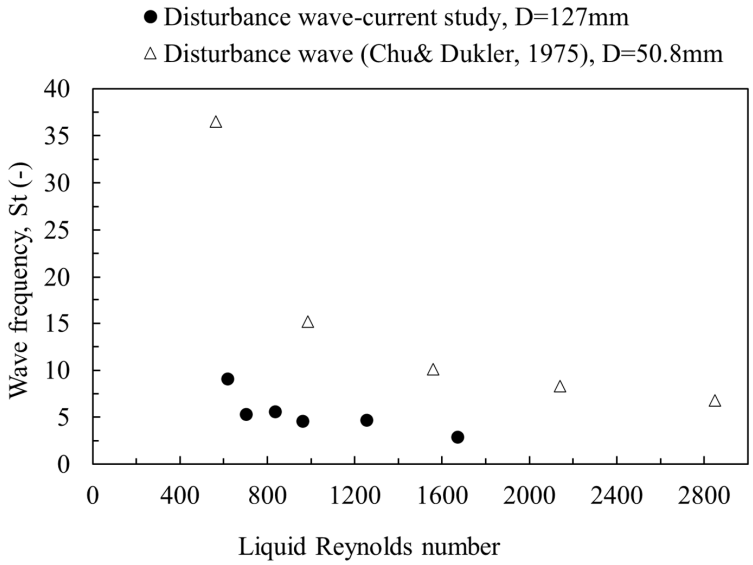

Figure 8. Effect of pipe diameter on disturbance wave frequency [31].

It is seen that the disturbance-wave frequency in the current study is lower compared to Chu and Dukler [31]. Furthermore, while the frequency of disturbance waves in Chu and Dukler's study is significantly affected by the liquid Reynolds number Re_L, it appears to be less sensitive to Re_L in the case of a 127 mm diameter pipe.

3.2. Wave Velocity

The waves, in the axial direction, were found to evolve with time and move approximately with constant velocity. Figure 9 shows the maximum cross-correlated time delay (τ) as a function of the axial distance or planes at fixed circumferential position. In this Figure, plane 6 is selected as a reference axial location (i.e., the *y*-axis value at axial distance '0 m' corresponds to the time delay τ(s) extracted from the film thickness time series between planes 6 and 6, while the *y*-axis value at axial location '0.077 m' corresponds to the cross correlation between planes 6 and 1). The data of τ(s) in Figure 9 can be linearly fitted which indicates that wave moves roughly at constant velocity. The velocity is simply a reciprocal of the slope of the line. In addition, as Re_L increases, the velocity of the waves increases (and hence the slope decreases).

Figure 10 shows the time delay-maximum cross correlation of circumferential film thickness data at a fixed axial location for Re_L = 618. As can be seen, the velocity of the wave in the circumferential direction is nearly zero and can be considered negligible.

The mean axial wave velocity increases with increasing Re_L, as shown in Figure 11a. Overall, the mean axial velocity does not vary much with circumferential position. However, at high Reynolds numbers, this uniformity is somewhat reduced, leading to a more noticeable variation. The plot also incorporates experimental data on mean wave velocity from Chu and Dukler [31] to emphasize the influence of pipe diameter on the mean axial wave velocity. It is evident that the wave travels slower in smaller pipe diameters. In smaller pipe diameters,

the interfacial waves seem to maintain greater coherence around the circumference, while in larger pipes, they are typically less coherent and more localized [25,31]. In addition, the influence of the pipe walls on the liquid film is more significant in smaller pipe diameters, which could enhance viscous forces and amplifies surface tension effects.

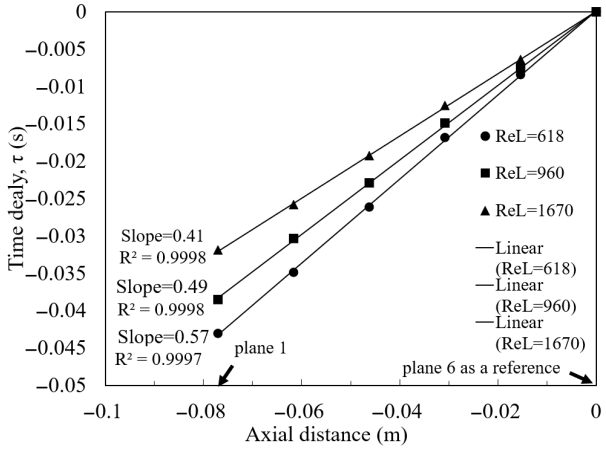

Figure 9. Time delay-maximum cross correlation of film thickness data in axial direction at fixed circumferential point (using plane 6 of MPFS as a reference axial location).

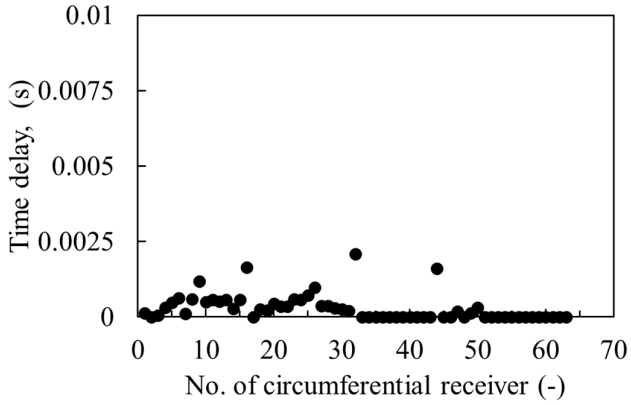

Figure 10. Time delay obtained from maximum cross correlation of film thickness data around the pipe at fixed axial position, Re_L = 618.

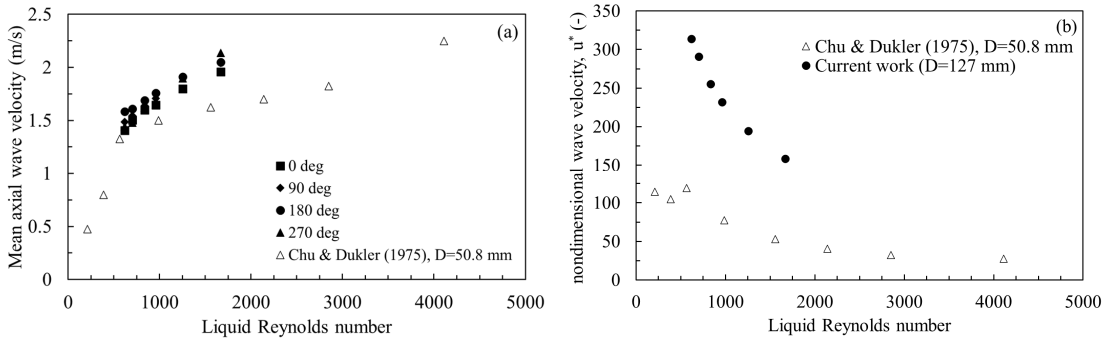

Figure 11. Comparison of (**a**) the mean axial wave velocity of the current work (ID = 127 mm) at different circumferential locations with the work by Chu & Dukler (ID = 50.8 mm), (**b**) the non-dimensional disturbance-wave velocity with the work by Chu and Dukler (ID = 50.8 mm), [31].

To better compare the effect of the pipe diameter on the wave velocity, a nondimensional disturbance-wave velocity, $u*$, is defined as follows:

$$u* = \frac{u_w \mathrm{D}}{Re_L\, \nu} \tag{3}$$

where u_w is the mean disturbance-wave velocity and ν is the kinematic viscosity of the liquid.

Figure 11b illustrates the effect of pipe diameter on the axial disturbance-wave velocity of a freely falling liquid film.

Although the resolution in the axial direction is limited, the MPFS was able to quantify large waves. Figure 12 illustrates the temporal–spatial (position–time) plot of the film thickness, showing how the large waves evolved with time and axial position (plane 1 to 9). As expected, it is seen that both wave number and wave magnitude increased with increasing $\mathrm{Re_L}$. In addition, it is clear that large waves in the falling liquid film move approximately with the same velocity (i.e., the slope of the line is approximately constant). This qualitative observation also confirms the results obtained in Figure 9 by a cross-correlation technique.

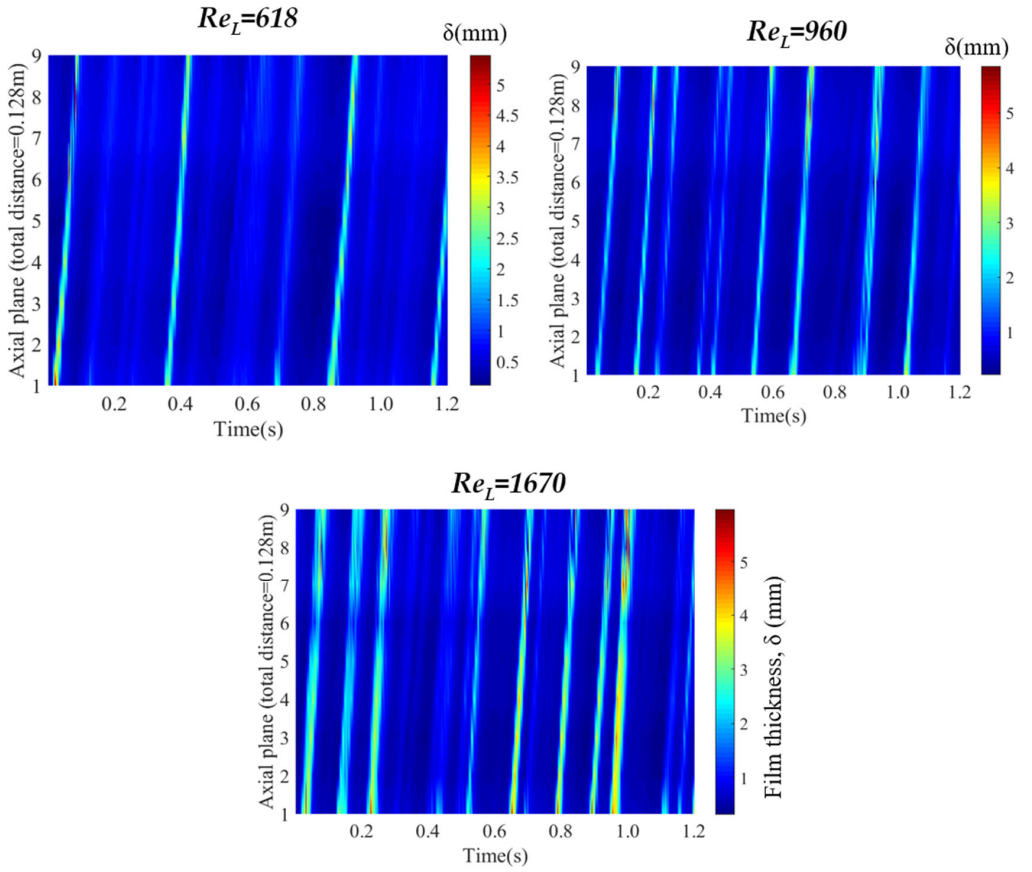

Figure 12. Reconstructed spatiotemporal images of film thickness at different values of liquid Reynolds number. The colour bar shows the velocity in (m/s).

3.3. Wave Spacing and Widths

Mean wave spacing and mean wave widths are estimated by defining the Minimum Peak Prominence (MPP) values, as mentioned earlier. Figure 13 shows an example of detecting the peaks of the waves extracted from the time series of one receiver (sensor) using MPP as $0.5\overline{\delta}$,$1.5\overline{\delta}$, $1\overline{\delta}$, $2\overline{\delta}$, $3\overline{\delta}$, and $4\overline{\delta}$, respectively ($\overline{\delta}$ is the average film thickness). The width of the wave was calculated at a half prominence length (i.e., at half of the wave amplitude). The wave widths were converted from the time domain to the spatial domain

using the wave velocity. The number of waves decreased as the MPP (and hence the factor that was multiplied by the mean film thickness) increased.

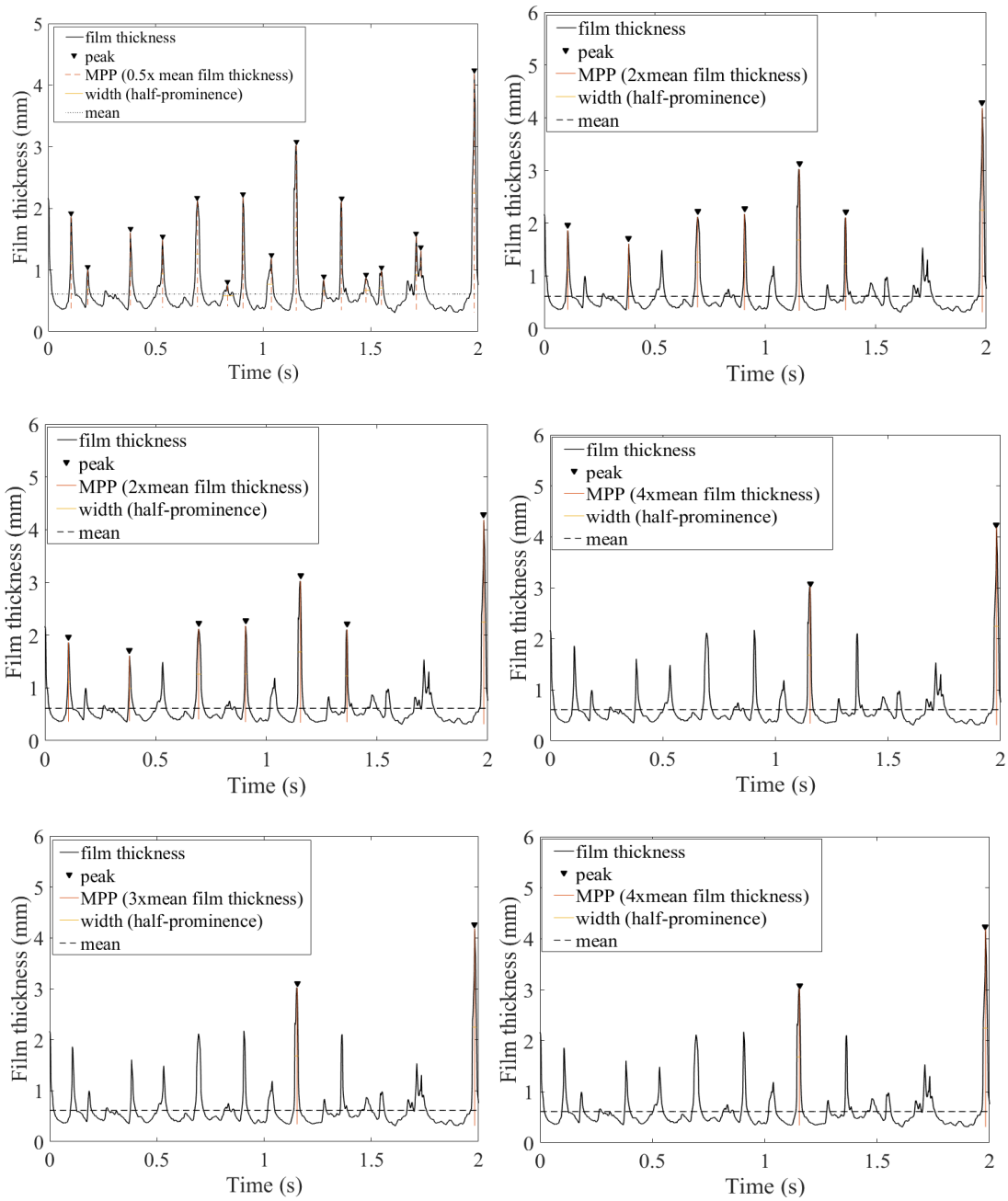

Figure 13. Peaks of the waves at liquid Reynolds number, Re_L = 618.

The relationship between the mean width of the waves and the liquid Reynolds number is shown in Figure 14. The mean width of the waves generally tends to increase with the liquid Reynolds number. For MPP = $4\bar{\delta}$ (a typical disturbance wave), the width of the waves starts to increase at low liquid Reynolds number, Re_L and then becomes approximately constant at higher liquid Reynolds number, showing that at $Re_L > 960$, the width of the disturbance waves seems to be independent of Re_L. This was also reported by [22]. The width and steepness of waves depend on the balance between the inertia force of the liquid film and the surface tension. An increase in inertia can cause the wave front to become steeper [42]. At low liquid Reynolds numbers (Re_L), viscous force and surface tension are dominant, causing the width of waves to increase. At high Re_L, a balance is

established between inertia (which tends to steepen the waves) and surface tension (which resists this steepening), resulting in a relatively constant width of the larger waves.

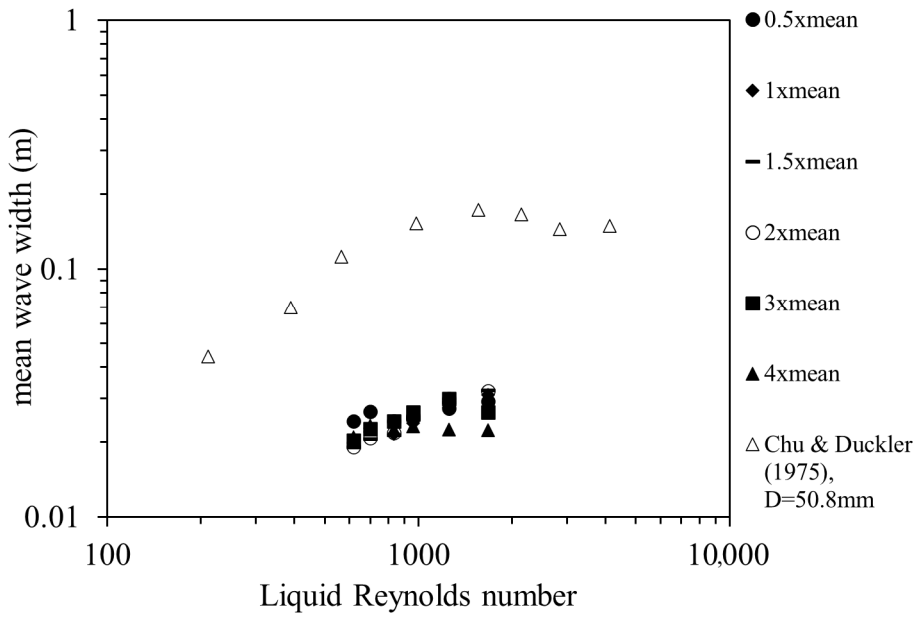

Figure 14. Mean width of the waves at different liquid Reynolds number [31].

The average width of disturbance waves in a free-falling film within a 50.8 mm diameter pipe [31] was observed to be greater compared to that in a larger pipe diameter (127 mm, as in this study). It should be noted that Chu and Dukler [31] measured the disturbance wave width based on the time of passage at the base wave, whereas in this study, the wave width was determined at half the height of the prominent peak (i.e., half the wave amplitude).

Sekoguchi and Mori [43] and Kondo et al. [22] found that the mean width of disturbance waves is approximately 2/3 of pipe diameters (i.e., 66.66% of pipe diameters). However, in this study, the mean wave width of the disturbance wave (i.e., 4 $\times\overline{\delta}$ data in Figure 14) at moderate-to-high liquid Reynolds number is approximately 17.7% of pipe diameter. It should be mentioned that the above two studies by Sekoguchi and Kondo were conducted for annular liquid–gas upward flows while in the current study, a free-falling liquid film was studied where the interfacial shear stresses caused by the gas flow being absent. In addition, a larger pipe diameter of 0.127 m was used in this study compared to [43], who used a pipe diameter of 0.026 m. The interfacial waves in small pipe diameters appear to be more coherent around the pipe circumference, whereas in larger pipes they are generally less coherent and tend to be more localized [25,32].

Figure 15 shows the effect of Re_L on the mean wave spacing. The wave spacing increases with increasing MPP value. This looks reasonable because when the minimum prominent peak MPP value is defined as 0.5 times the mean film thickness, a large number of small waves over the substrate surface are counted, while, for MPP = $4\overline{\delta}$, where large waves are only considered, less frequent waves exist. For the liquid Reynolds number $Re_L > 835$ and MPP = $0.5\overline{\delta}$, $1\overline{\delta}$, $1.5\overline{\delta}$, $2\overline{\delta}$, and $3\overline{\delta}$, it appears that the wave spacing is almost independent of Re_L. However, for MPP = $4\overline{\delta}$ (i.e., a typical disturbance wave), it generally appears that the mean wave spacing decreased with increasing liquid Reynolds number. This could be due to the waves coalescence to form large waves at higher Re_L [39,40].

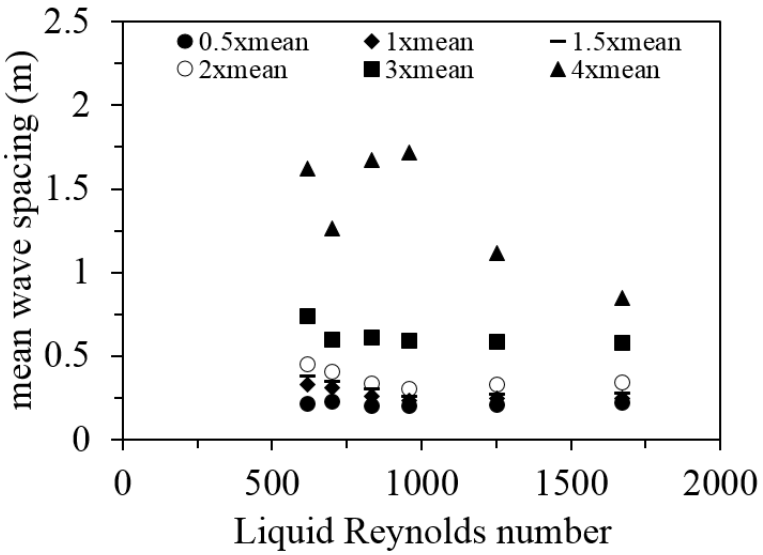

Figure 15. Effect of liquid Reynolds number, Re_L, on the mean wave spacing.

The effect of Re_L on the wave peaks at different MPP values is shown in Figure 16. The mean wave peaks increased as the liquid Reynolds number, Re_L, increased. This increase in Re_L results in more wave development and coalescence, leading to the formation of additional large waves. In addition, the number of capillary ripples preceding a wave hump increases with increasing Reynolds number [42,44,45]. When comparing the current data (obtained with a 127 mm pipe diameter) to that of Chu and Dukler (who measured large waves using a 50.8 mm pipe), it is evident that the mean wave amplitude is significantly more pronounced in larger pipe diameters than in smaller ones.

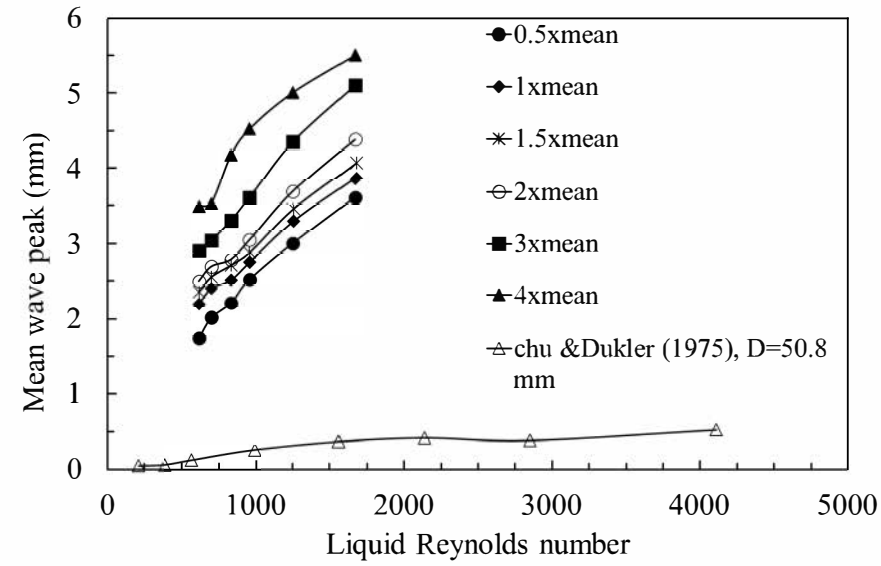

Figure 16. Effect of Re_L on the mean wave peak at different MPP values [31].

4. Conclusions

This paper presents an experimental investigation of wavy liquid film behaviour, focusing on wave frequency, velocity, width, and spacing. The disturbance-wave PSD exhibits a pronounced peak at 6–8 Hz, consistent with prior studies (e.g., Chu and Dukler [31] and Takahama and Kato [35]). The occurrence of disturbance waves is nearly independent of the liquid Reynolds number, in agreement with Karapantsios et al. [11].

Cross-correlation results indicate downstream propagation at an approximately constant axial velocity, with mean axial wave speed increasing with Reynolds number, while the mean circumferential wave velocity remains approximately zero. With increasing Reynolds number, both wave magnitude and wave number increase; the mean disturbance-wave width rises at low Reynolds numbers and becomes nearly constant at higher Reynolds numbers, averaging to about 17.7% of the pipe diameter. Pipe diameter has a strong effect in which the 50.8 mm pipe shows a substrate-wave frequency ~3.5 times that of the 127 mm pipe and more frequent large waves, but lower mean axial wave velocity and amplitude, alongside a larger mean wave width.

Author Contributions: Conceptualization, B.J.A., A.H.H. and B.H.; methodology, A.H.H., S.K.M. and B.J.A.; software, A.H.H. and S.K.M.; validation, A.H.H., S.K.M. and F.S.; formal analysis, A.H.H.; investigation, A.H.H. and S.K.M.; data curation, A.H.H., S.K.M. and A.A.; writing—original draft preparation, A.H.H., S.K.M., F.S. and A.A.; writing—review and editing, A.H.H., S.K.M., B.H., F.S. and A.A.; visualization, A.H.H. and S.K.M. All authors have read and agreed to the published version of the manuscript.

Funding: EPSRC through the MEMPHIS grant (EP/K003976/1).

Data Availability Statement: The data and original contributions are both included in the article. Additional details can be requested directly from the corresponding author.

Conflicts of Interest: The authors declare no conflicts of interest.

References

1. Bouyahiaoui, H.; Azzi, A.; Zeghloul, A.; Hasan, A.H.; Al-Sarkhi, A.; Parsi, M. Vertical upward and downward churn flow: Similarities and differences. *J. Nat. Gas Sci. Eng.* **2020**, *73*, 103080. [CrossRef]
2. Al-Aufi, Y.; Hewakandamby, B.; Dimitrakis, G.; Holmes, M.; Hasan, A.; Watson, N. Thin film thickness measurements in two phase annular flows using ultrasonic pulse echo techniques. *Flow Meas. Instrum.* **2019**, *66*, 67–78. [CrossRef]
3. Hasan, A.H.; Mohammed, S.K.; Pioli, L.; Hewakandamby, B.N.; Azzopardi, B.J. Gas rising through a large diameter column of very viscous liquid: Flow patterns and their dynamic characteristics. *Int. J. Multiph. Flow* **2019**, *116*, 1–14. [CrossRef]
4. Mohammed, S.K.; Hasan, A.H.; Ibrahim, A.; Dimitrakis, G.; Azzopardi, B.J. Dynamics of flow transitions from bubbly to churn flow in high viscosity oils and large diameter columns. *Int. J. Multiph. Flow* **2019**, *120*, 103095. [CrossRef]
5. Mohammed, S.K.; Hasan, A.; Dimitrakis, G.; Azzopardi, B.J. Churn flow in high viscosity oils and large diameter columns. *Int. J. Multiph. Flow* **2018**, *100*, 16–29. [CrossRef]
6. Dukler, A. The Role of Waves in Two Phase Flow: Some New Understandings. In *Chemical Engineering Education*; U.S. Nuclear Regulatory Commission: Rockville, MA, USA, 1977.
7. Dukler, A. Characterization, effects and modeling of the wavy gas-liquid interface. *Prog. Heat Mass Transf.* **1972**, *6*, 207.
8. Emmert, R. A study of gas absorption in falling liquid films. *Chem. Eng. Prog.* **1954**, *50*, 87–93.
9. Telles, A.S.; Dukler, A.E. Statistical characteristics of thin, vertical, wavy, liquid films. *Ind. Eng. Chem. Fundam.* **1970**, *9*, 412–421. [CrossRef]
10. Gjevik, B. Occurrence of Finite-Amplitude Surface Waves on Falling Liquid Films. *Phys. Fluids* **1970**, *13*, 1918–1925. [CrossRef]
11. Karapantsios, T.; Paras, S.; Karabelas, A. Statistical characteristics of free falling films at high Reynolds numbers. *Int. J. Multiph. Flow* **1989**, *15*, 1–21. [CrossRef]
12. Zadrazil, I.; Matar, O.K.; Markides, C.N. An experimental characterization of downwards gas–liquid annular flow by laser-induced fluorescence: Flow regimes and film statistics. *Int. J. Multiph. Flow* **2014**, *60*, 87–102. [CrossRef]
13. Gerke, S.J.; Repke, J.-U. Experimental investigations of the fluid dynamics in liquid falling films over structured packing geometry. *Chem. Eng. Res. Des.* **2019**, *147*, 634–643. [CrossRef]
14. Zeng, J.; Wang, Y.; Wei, Z.; Wang, L.; Li, T.; Yu, G. Thickness distribution and fluctuation characteristics of liquid falling film under turbulent conditions. *Chem. Eng. Sci.* **2022**, *248*, 117172. [CrossRef]
15. Meza, C.E.; Balakotaiah, V. Modeling and experimental studies of large amplitude waves on vertically falling films. *Chem. Eng. Sci.* **2008**, *63*, 4704–4734. [CrossRef]

16. Yu, Y.; Wei, S.; Yang, Y.; Cheng, X. Experimental study of water film falling and spreading on a large vertical plate. *Prog. Nucl. Energy* **2012**, *54*, 22–28. [CrossRef]
17. Drosos, E.; Paras, S.; Karabelas, A. Characteristics of developing free falling films at intermediate Reynolds and high Kapitza numbers. *Int. J. Multiph. Flow* **2004**, *30*, 853–876. [CrossRef]
18. Karapantsios, T.; Karabelas, A. Longitudinal characteristics of wavy falling films. *Int. J. Multiph. Flow* **1995**, *21*, 119–127. [CrossRef]
19. Karimi, G.; Kawaji, M. An experimental study of freely falling films in a vertical tube. *Chem. Eng. Sci.* **1998**, *53*, 3501–3512. [CrossRef]
20. Pavlov, D.; Gurbatov, S.; Kudryashov, S.; Gurevich, E.; Kuchmizhak, A. Laser-induced surface relief nanocrowns as a manifestation of nanoscale Rayleigh-Plateau hydrodynamic instability. *Appl. Surf. Sci.* **2020**, *511*, 145463. [CrossRef]
21. Chao, Y.; Lu, Y.; Yuan, H. On reactive thin liquid films falling down a vertical cylinder. *Int. J. Heat Mass Transf.* **2020**, *147*, 118942. [CrossRef]
22. Kondo, Y.; Mori, K.; Yagishita, T.; Nakabo, A. Effect of liquid viscosity on wave behaviour in gas-liquid two-phase flow. In Proceedings of the 5th ASME/JSME Joint Thermal Engineering, San Diego, CA, USA, 15–19 March 1999.
23. Hewitt, G.F.; Nicholls, B. *Film Thickness Measurement in Annular Two-Phase Flow Using a Fluorescence Spectrometer Technique. Part II. Studies of the Shape of Disturbance Waves*; Atomic Energy Research Establishment: Harwell, UK, 1969.
24. Pashniak, D.W. *An Investigation of the Interfacial Disturbances in Vertical Two Phase Flow*; University of Washington: Seattle, WA, USA, 1969.
25. Azzopardi, B. Disturbance wave frequencies, velocities and spacing in vertical annular two-phase flow. *Nucl. Eng. Des.* **1986**, *92*, 121–133. [CrossRef]
26. Belt, R.; Westende, J.V.; Prasser, H.; Portela, L. Time and spatially resolved measurements of interfacial waves in vertical annular flow. *Int. J. Multiph. Flow* **2010**, *36*, 570–587. [CrossRef]
27. Wolf, A.; Jayanti, S.; Hewitt, G. Flow development in vertical annular flow. *Chem. Eng. Sci.* **2001**, *56*, 3221–3235. [CrossRef]
28. Zeghloul, A.; Azzi, A.; Hasan, A.; Azzopardi, B.J. Behavior and pressure drop of an upwardly two-phase flow through multi-hole orifices. *Proc. Inst. Mech. Eng. Part C J. Mech. Eng. Sci.* **2017**, *232*, 3281–3299. [CrossRef]
29. Chu, K.J.; Dukler, A.E. Statistical characteristics of thin, wavy films: Part II. Studies of the substrate and its wave structure. *AIChE J.* **1974**, *20*, 695–706. [CrossRef]
30. Hewitt, G.F.; Lovegrove, P. *Frequency and Velocity Measurements of Disturbance Waves in Annular Two-Phase Flow*; Atomic Energy Research Establishment: Harwell, UK, 1969.
31. Chu, K.J.; Dukler, A.E. Statistical characteristics of thin, wavy films III. Structure of the large waves and their resistance to gas flow. *AIChE J.* **1975**, *21*, 583–593. [CrossRef]
32. Hasan, A.H.; Mohammed, S.K.; Hewakandamby, B.; Azzopardi, B. Experimental study of the three-dimensional interfacial wave structure of freely falling liquid film in a vertical large pipe diameter. *Chem. Eng. Res. Des.* **2021**, *169*, 66–76. [CrossRef]
33. Chu, K. Statistical characterisation and modelling of wavy liquid films in vertical two-phase flow. In *Chemical Engineering*; University of Houston: Houston, TX, USA, 1973.
34. Whalley, P.B.; GFHewitt Hutchinson, P. *Experimental Wave and Entrainment Measurements in Vertical Annular Two-Phase Flow*; Atomic Energy Research Establishment: Harwell, UK, 1973.
35. Takahama, H.; Kato, S. Longitudinal flow characteristics ofvertically falling liquid films without concurrent gas flow. *Int. J. Multiph. Flow* **1980**, *6*, 203–215. [CrossRef]
36. Zabaras, G.; Dukler, A.E.; Moalem-Maron, D. Vertical upward cocurrent gas-liquid annular flow. *AIChE J.* **1986**, *32*, 829–843. [CrossRef]
37. Azzopardi, B. Drops in annular two-phase flow. *Int. J. Multiph. Flow* **1997**, *23*, 1–53. [CrossRef]
38. Adomeit, P.; Renz, U. Hydrodynamics of three-dimensional waves in laminar falling films. *Int. J. Multiph. Flow* **2000**, *26*, 1183–1208. [CrossRef]
39. Wei, Z.; Wang, Y.; Wu, Z.; Peng, X.; Yu, G. Wave characteristics of the falling liquid film in the development region at high Reynolds numbers. *Chem. Eng. Sci.* **2020**, *215*, 115454. [CrossRef]
40. Denner, F.; Charogiannis, A.; Pradas, M.; Markides, C.N.; van Wachem, B.G.M.; Kalliadasis, S. Solitary waves on falling liquid films in the inertia-dominated regime. *J. Fluid Mech.* **2018**, *837*, 491–519. [CrossRef]
41. Song, J.; Hu, P.; Wei, S.J.; Yu, Y.Q.; Yang, Y.H. Experimental study on surface wave evolution behavior of water film falling down vertical plate. *At. Energy Sci. Technol.* **2012**, *46*, 804–808.
42. Denner, F.; Pradas, M.; Charogiannis, A.; Markides, C.N.; van Wachem, B.G.M.; Kalliadasis, S. Self-similarity of solitary waves on inertia-dominated falling liquid films. *Phys. Rev. E* **2016**, *93*, 033121. [CrossRef]
43. Sekoguchi, K.; Mori, K. New development of experimental study on interfacial structure in gas-liquid two-phase flow. *Exp. Heat Transf. Fluid Mech. Thermodyn.* **1997**, *2*, 1177–1188.

44. Nosoko, T.; Yoshimura, P.; Nagata, T.; Oyakawa, K. Characteristics of two-dimensional waves on a falling liquid film. *Chem. Eng. Sci.* **1996**, *51*, 725–732. [CrossRef]
45. Pradas, M.; Tseluiko, D.; Kalliadasis, S. Rigorous coherent-structure theory for falling liquid films: Viscous dispersion effects on bound-state formation and self-organization. *Phys. Fluids* **2011**, *23*, 044104. [CrossRef]

Disclaimer/Publisher's Note: The statements, opinions and data contained in all publications are solely those of the individual author(s) and contributor(s) and not of MDPI and/or the editor(s). MDPI and/or the editor(s) disclaim responsibility for any injury to people or property resulting from any ideas, methods, instructions or products referred to in the content.